

## MEASUREMENTS OF LOW FREQUENCY NOISE OF INFRARED PHOTO-DETECTORS WITH TRANSIMPEDANCE DETECTION SYSTEM

Łukasz Ciura<sup>1</sup>), Andrzej Kolek<sup>1</sup>), Waldemar Gawron<sup>2</sup>), Andrzej Kowalewski<sup>2</sup>),  
Dariusz Stanaszek<sup>3</sup>)

1) Rzeszów University of Technology, Department of Electronic Fundamentals, al. Powstańców Warszawy 12, 35-959 Rzeszów, Poland (✉ ciura.lukasz@gmail.com, 669212770)

2) Institute of Applied Physics, Military University of Technology, 2 Kaliskiego St., 00-908 Warsaw, Poland (wgawron@wat.edu.pl, +48 22 6839673)

3) Vigo System S.A., 129/133 Poznańska Str., 05-850 Ożarów Mazowiecki, Poland (dstanaszek@vigo.com.pl, +48 22 6839673)

### Abstract

The paper presents the method and results of low-frequency noise measurements of modern mid-wavelength infrared photodetectors. A type-II InAs/GaSb superlattice based detector with nBn barrier architecture is compared with a high operating temperature (HOT) heterojunction HgCdTe detector. All experiments were made in the range 1 Hz - 10 kHz at various temperatures by using a transimpedance detection system, which is examined in detail. The power spectral density of the nBn's dark current noise includes Lorentzians with different time constants while the HgCdTe photodiode has more uniform  $1/f$ -shaped spectra. For small bias, the low-frequency noise power spectra of both devices were found to scale linearly with bias voltage squared and were connected with the fluctuations of the leakage resistance. Leakage resistance noise defines the lower noise limit of a photodetector. Other dark current components give raise to the increase of low-frequency noise above this limit. For the same voltage biasing devices, the absolute noise power densities at 1 Hz in nBn are 1 to 2 orders of magnitude lower than in a MCT HgCdTe detector. In spite of this, low-frequency performance of the HgCdTe detector at  $\sim 230\text{K}$  is still better than that of InAs/GaSb superlattice nBn detector.

Keywords:  $1/f$  noise, infrared detectors, nBn structure, HgCdTe heterostructure, noise measurements, transimpedance detection system, type-II InAs/GaSb superlattice.

© 2014 Polish Academy of Sciences. All rights reserved

### 1. Introduction

Recently a new generation of infrared (IR) detectors tries to compete with traditional high operating temperature (HOT) Mercury-Cadmium-Telluride (MCT) devices. They utilize II-type superlattice (T2SL) what enables continuous tuning of wavelength cutoff maintaining high uniformity required for focal plane arrays (FPAs) as well as a barrier architecture which strongly reduces dark current. Due to these efforts, the performance of barrier T2SL detectors achieves the level of MCT detectors. While the comparison of detectors' performance bases on the usual figures of merit like detectivity or  $R_0A$  product and refers to a frequency range high enough to justify the use of thermal or shot noise limitation, the performance of IR detectors for slowly varying signals is less experienced. Contrary to the high-frequency value which bases on theoretical estimates of Johnson or Schottky [1], the low-frequency ( $1f$ ) detectivity requires direct measurements in the range where structural  $1/f$  noise dominates and must be taken into account, as novel detectors usually require bias for best operation. At present such studies with respect to T2SL detectors are merely being started and few papers deal with this issue [2, 3]. In addition, there is lack of papers that compare  $1f$  performance of T2SL and MCT detectors. The main purpose of this study is to provide such a comparison:  $1f$  noise properties of the nBn detector, which is an important example of T2SL detectors family,

are compared to a novel heterostructure MCT detector. We also draw some general conclusions concerning the origin of the  $1/f$  noise in these devices. Our analysis bases on experimental data on nBn devices and measurements of the MCT device described in Sec. 2. This section follows Sec. 1, where devices compared in this study are introduced. An important contribution of our study is also the detailed analysis of noise measurements made with a transimpedance detection system.

## 2. Devices

The nBn detector was manufactured in the Center for High Technology Materials, University New Mexico in Albuquerque [4-6]. Its architecture is shown in Fig. 1. It was grown on type n GaSb substrate (001) using MBE technology. In nBn architecture, the barrier appears only in the conduction band and blocks electrons while the holes flow with no impedance. The n.i.d.  $\text{Al}_{0.2}\text{Ga}_{0.8}\text{Sb}$  barrier is thick enough to prevent direct tunneling between the upper contact layer and the absorber. The superlattice material used in this device consists of 10 monolayers (ML) of InAs and 10 ML of GaSb repeated a number of times. Namely, the n-type absorber and contact layers contain 320 and 25 SL periods respectively. With this SL design the 50% cut-off wavelength was tuned to the mid-wavelength infrared (MWIR) value of  $\lambda = 4.5 \mu\text{m}$  at 77 K. The detector area is  $A = 1.68 \times 10^{-3} \text{ cm}^2$ .

The heterostructure HgCdTe detector was grown by MOCVD technology in VIGO System laboratories. Its architecture and more detailed information about Hg/Cd contents and thickness of the layers are shown in Fig. 1. The detector was grown on GaAs substrate with CdTe as buffer layer. Successive layers form the heterostructure photodiode. Capital letters denote layers with greater bandgap (higher content of Cd). The sign „+” denotes higher doping concentration. Layer  $\text{N}^+$  is I doped while the absorber and P, P+ layers are As doped. The CdTe passivation was used. The detector area is  $A = 1.2 \times 10^{-3} \text{ cm}^2$ . A full description of this structure which was optimized for HOT conditions can be found elsewhere, e.g. in ref. [7].

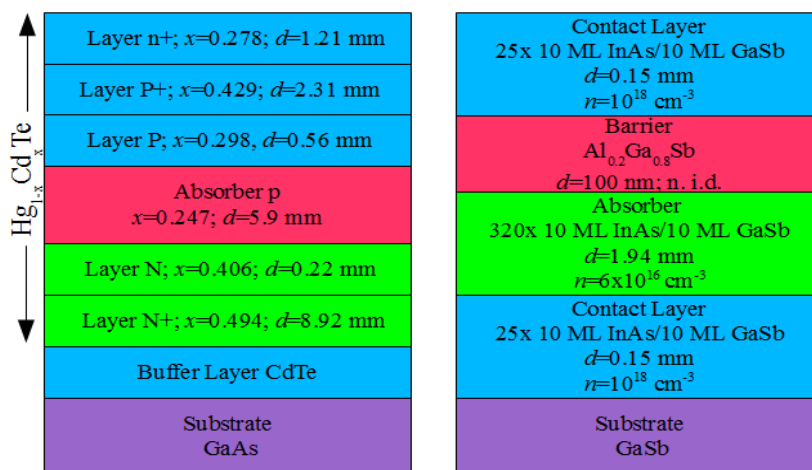


Fig.1. Architecture of MCT heterostructure photodiode (left) and nBn T2SL (right) detectors.

Basic electrical characteristics of nBn and MCT detectors measured at 77 K are depicted in Fig. 2. Namely, dark current  $I_D$  and the product  $RA$ , where  $R$  is the differential (dynamic) resistance are plotted as a function of bias voltage  $U_D$ .  $R$  was calculated by graphical

differentiation of the I-V curve. For both devices, the forward direction ( $U_D > 0$ ) is defined for the bias voltages that give larger dark current magnitudes. In the low voltage limit, all I-V curves are linear. For the nBn detector this low-bias ohmic-like behavior, characterized by the leakage (shunt) resistance of  $R_{\text{leak}} = 1.5 \text{ M}\Omega$ , results probably from the surface leakage. This kind of leakage is extremely sensitive to passivation and etching processes [4, 5] especially for single mesa devices, which is the case of our specimen. Many studies report on surface leakage in T2SL detectors operating at  $\sim 5 \text{ }\mu\text{m}$  wavelength, including nBn's [1], p-n diodes [6] and complementary barrier devices (barriers in conduction and valence bands) [8]. The origin of ohmic-like behavior in MCT diodes is not well recognized. Many authors indicate that dislocations in bulk HgCdTe are the main source of leakage current [9, 10, 11]. Their conclusion relies on a significant correlation found between dislocation density and the magnitude of the leakage current (as well as  $1/f$  noise). On the other hand, correlation between  $1/f$  noise/leakage current ratio and perimeter was found at room temperature [12]. This suggests surface origin of  $1/f$  noise in HOT MCT diodes. For our MCT detector the low-bias behavior at 77 K is quantitatively characterized by the leakage resistance of  $R_{\text{leak}} = 38 \text{ k}\Omega$ .

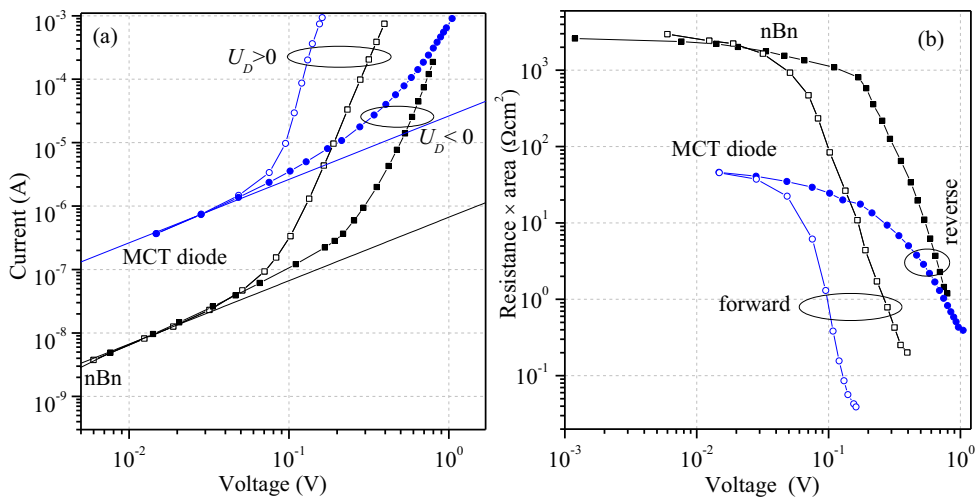


Fig. 2. Dark current (a) and product  $RA$  (b) versus forward (empty symbols) and reverse (filled symbols) bias voltage for the nBn detector and the photodiode (circles). Lines indicate an ohmic component with the leakage resistance  $R_{\text{leak}} = 38 \text{ k}\Omega$  for MCT diode or  $R_{\text{leak}} = 1.5 \text{ M}\Omega$  for nBn.

The crossover to nonlinear behavior is observed near  $|U_D| \approx 0.1 \text{ V}$ . Nonlinear I-V dependence can be attributed to trap-assisted and band-to-band tunneling that dominate dark current in nBn at 77 K [1]. In the heterostructure p-n junction the trap-assisted tunneling dominates for reverse bias  $U_D < -0.1 \text{ V}$  (Fig. 2a) while for the forward bias generation-recombination prevails. Consequently, data follow the relation  $I_D \sim \exp(qU_D/2kT)$  for  $U_D > 0$ . Band-to-band tunneling current is probably absent in our MCT detector in the voltage range of interest. Cd content  $x = 0.247$  corresponds to material bandgap of  $E_g = 0.16 \text{ eV}$  while experiments with MCT p-n homojunction detectors performed at 80 K show that band-to-band tunneling is absent down to  $U_D = -1 \text{ V}$  when  $x = 0.32$  ( $E_g \approx 0.26 \text{ eV}$ ) [13] or  $U_D = -0.4 \text{ V}$  when  $x = 0.22$  ( $E_g = 0.115 \text{ eV}$ ) [14].

At 77 K a small-bias dark current of the nBn detector is much lower than that of the HgCdTe diode. This translates for much better deflection performance. With no bias the product  $RA \equiv R_0A = 2600 \text{ }\Omega\text{cm}^2$  calculated for nBn is much larger than  $R_0A = 45.5 \text{ }\Omega\text{cm}^2$

calculated for the photodiode. The situation changes dramatically when we turn to higher temperatures  $> 200$  K. Namely,  $R_0A = 0.1 \Omega\text{cm}^2$  for nBn as compared to  $R_0A = 0.7 \Omega\text{cm}^2$  for MCT detector, both measured at  $\sim 230$  K. These numbers illustrate the current stage of development of new generation T2SL detectors for high HOT implementations – their performance, while approaching photodiode HOT HgCdTe devices, still needs to be improved.

### 3. Method of noise measurements

The noise of a photodetector is usually specified in terms of noise current spectra and/or related wideband measures. The setup for direct measurements of noise current is shown in Fig. 3a. Attenuator  $R_1/R_2$  provides a dc bias. The entire detector current  $i_D$  comprises ac noise and signal currents and dc bias current  $I_D$ . The large-value capacitor  $C$  creates a path for all ac signals. Efficiency of this shorting is controlled by the measurement of coherence function between the fluctuations of detector’s voltage and current. These fluctuations are measured with low noise amplifiers: EG&G 5182 (W1) and EG&G 5186 (W2). Device W1 is a variable gain transimpedance amplifier. Its output voltage  $U_{out}$  is proportional to input ac current  $i$ ,  $U_{out} = k_{iu}i$  where  $k_{iu}$  is the transimpedance gain. Device W2 is a low-noise voltage ( $\times 1000$ ) amplifier. When capacitor  $C$  effectively shorts ac signals to the ground, the ac component of bias voltage zeroes and so the coherence function mentioned above.

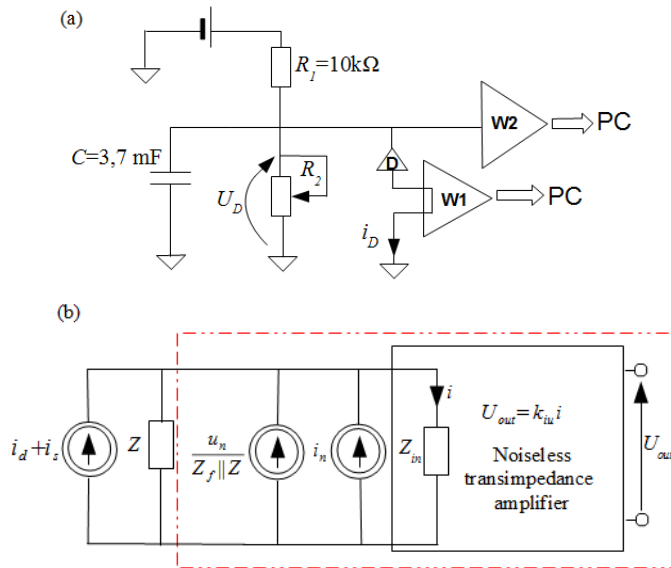


Fig. 3. Measurement setup of a photodetector (D) noise current (a). Noise model of the measurement setup of figure (a) with EG&G 5182 unit as transimpedance amplifier W1 (b).

The output voltage  $U_{out}$  is disturbed by internal noise of amplifier W1. The noise model of the detection system in Fig. 3a with an EG&G 5182 unit which uses feedback OP-amp implementation is shown in Fig. 3b. It contains amplifier equivalent input noise sources  $i_n$  and  $u_n$ , as well as the feedback and input impedances  $Z_f$ ,  $Z_{in}$ .  $Z$  represents device impedance in parallel with the test fixture impedance, which usually introduces only a capacitive contribution. The leftmost current source represents device noise  $i_d$  to be measured and noise  $i_s$  connected with the optical signal. In “dark” measurements  $i_s$  contains only the noise

generated by background thermal radiation. In our experiments both the background and the device were kept at the same temperature and so  $i_s$  can be neglected because for  $T < 230$  K and  $\lambda \approx 5 \mu\text{m}$  it is much lower than device's related noise  $i_d$ .

Provided  $|Z_{in}| \ll |Z|$ , which is also a condition for efficient signal detection, the total current amplified/measured in the circuitry of Fig. 3b

$$i \cong i_n + \frac{u_n}{Z_f \parallel Z} + i_d, \quad (1)$$

contains several noise contributions. In the low-frequency range considered in this study the impedances may be replaced with their real contributions i.e.  $Z_f = R_f$ ,  $Z = R$ . With these substitutions and switching to power spectral densities (psd) (1) can be rewritten as:

$$S_i = S_{in} + S_{id} + S_{un}/(R \parallel R_f)^2 + S_{inum}/(R \parallel R_f)^2, \quad (2)$$

where  $S_{inum}$  is the cross-power spectral density between signals  $i_n(t)$ ,  $u_n(t)$ . For the EG&G 5182 amplifier  $i_n$  and  $u_n$  are uncorrelated and so  $S_{inum} = 0$ . It stems from (2) that an important issue when measuring detector's noise is the identification of psds  $S_{in}$ ,  $S_{um}$  related to amplifier internal noise as well as a detector's differential resistance.  $S_{in}$  and  $S_{um}$  can be estimated by independent measurements for two different values of source resistance  $R_S$  connected to the amplifier's input. In equilibrium, resistance  $R_S$  generates exclusively thermal (Johnson) noise and so

$$S_i = S_{in} + 4kT/R_S + S_{un}/(R_S \parallel R_f)^2. \quad (3)$$

In the second experiment with open input amplifier ( $R_S = \infty$ )

$$S_i = S_{in} + S_{un}/R_f^2 \cong S_{in}. \quad (4)$$

From (3) and (4)  $S_{un}$  and  $S_{in}$  can be easily calculated as the feedback resistance is known. In Fig. 4 the estimated psds  $S_{un}(f)$  and  $S_{in}(f)$  are shown. As can be seen, the EG&G 5182 amplifier offers  $S_{un}(f) \approx 10^{-17} \text{ V}^2/\text{Hz}$  at the flat part of the spectrum which extends above 10 Hz and  $S_{in}(f)$  in the range  $2 \times 10^{-27} \div 1 \times 10^{-20} \text{ A}^2/\text{Hz}$  depending on the gain  $k_{iu}$ . The spectrum  $S_{in}$  is frequency dependent with a flat part above 10 Hz for  $k_{iu}=10^8$ ,  $10^7$  and above 100 Hz for  $k_{iu}=10^6$ . As expected,  $S_{in}$  depends on  $k_{iu}$  because the major contribution to  $i_n$  originates from thermal noise of the feedback resistor  $R_f$  which differs for different  $k_{iu}$ . On the other hand,  $S_{un}$  is described by internal OP-amp noise and so it is gain independent.

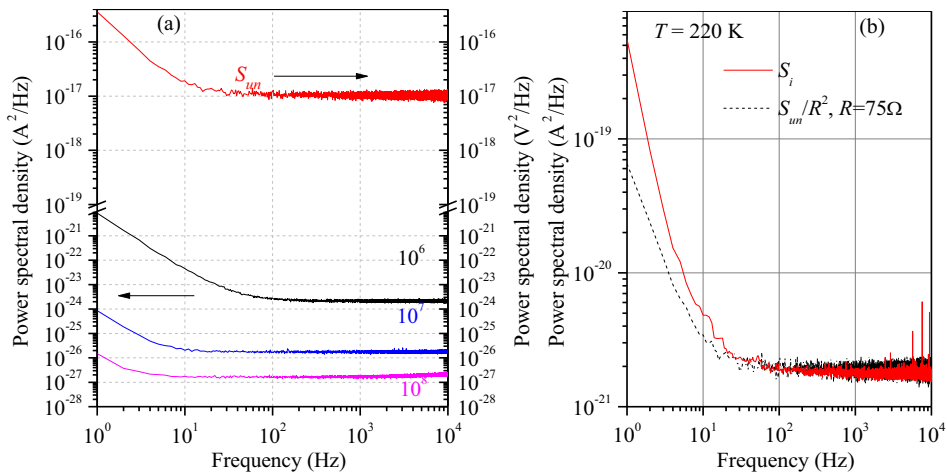


Fig. 4. Power spectral densities of amplifier EG&G 5182 noise sources  $S_{um}$  and  $S_{in}$  (a). Power spectral density of the noise current  $i$  measured for the reverse-biased ( $U_D = -0.013$  V,  $I_D = -0.17$  mA) nBn detector at  $T = 220$  K (solid red) compared to the background noise estimated for device dynamic resistance  $R = 75 \Omega$  (dashed black) (b).

The differential (dynamic) resistance of the photodetecting device, which enters formula (2) may occur crucial in case of low-differential-resistance sources. This case is illustrated in Fig. 4b where psd  $S_i$  measured for nBn detector reverse-biased to get  $R \approx 75 \Omega \ll R_f$  is shown. For  $f > 20$  Hz,  $S_i$  is completely dominated by the factor  $S_{um}/R^2$  which is also shown for the comparison. In such case, a detection of device's noise  $i_d$  is hardly possible. A reasonable accuracy of  $S_{id}$  estimator can be achieved only if it exceeds the instrumental background noise

$$S_{bg} \equiv S_{in}(f) + S_{um}/(R \parallel R_f)^2, \tag{5}$$

which must not be mistaken with the background thermal radiation noise which is negligible in our measurements. With this definition, it is possible to determine the minimum magnitude of device noise  $S_{id}$  suitable for measurements for specified dynamic resistance, frequency and amplifier gain. This is illustrated in Fig. 5 where  $S_{in}$ ,  $S_{um}(f)/R^2$  and  $S_{um}/(R \parallel R_f)^2$  are plotted versus device dynamic resistance. All quantities refer to the frequency of  $f = 100$  Hz at which the amplifier equivalent input noise sources become frequency independent. The dashed lines are the plots of  $S_{um}/R^2$  and  $S_{um}/(R \parallel R_f)^2$  with gain dependent value of resistance  $R_f = 10^4 \Omega$  ( $k_{iu} = 10^6$ ) or  $R_f = 10^6 \Omega$  ( $k_{iu} = 10^7$ ). As at higher frequencies  $S_{um}$  is frequency independent (see Fig. 4a) these curves remain unchanged for frequencies  $> 100$  Hz. Below this frequency, curve measurement of  $S_{id}(f)$  is hampered or not possible. The term  $S_{in}$  introduces an additional limit at higher values of dynamic resistance. Lines show this limit for various amplifier gains. One can observe that feedback resistance is negligible in estimating instrumental background noise because it is relevant only for large values of  $R$  where otherwise  $S_{in}$  dominates. Thus, the formula for the background noise simplifies to  $S_{in}$  for high values of detectors resistance and to  $S_{um}/R^2$  for low  $R$ -values. Namely,  $S_{um}/R^2$  becomes the major instrumental background noise contribution when the dynamic resistance gets lower than 2 k $\Omega$ ; 25 k $\Omega$ ; 80 k $\Omega$  for  $k_{iu} = 10^6$ ,  $10^7$ ,  $10^8$ , respectively. This limitation is particularly important at high temperatures and forward bias when the detector's dynamic resistance drops to very low values. At low temperatures and for the reverse biased devices the instrumental background noise contribution  $S_{in}$  plays a major role due to the high value of dynamic resistance in these circumstances.

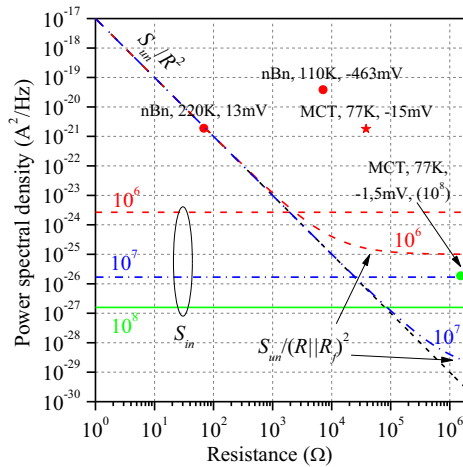


Fig. 5. Background noise components  $S_{in}/R^2$ ,  $S_{in}/(R|R|)^2$  and  $S_{in}$  at  $f = 100$  Hz versus dynamic resistance  $R$  of the photodetector. Colors/line styles refer to different transimpedance gain  $k_{iu} = 10^6$  (red/dashed),  $10^7$  (blue/dashed-dotted),  $10^8$  (green/solid). Dots and star represent measured values of  $S_i(f = 100$  Hz). Device, temperature, bias and gain (unless  $10^6$ ) are given for each measurement.

Symbols in the plot area refer to the values of total noise  $S_i$  measured for nBn and MCT devices at different bias, temperatures and gain. According to Fig. 4b the value  $S_i \approx 2 \times 10^{-21}$  A<sup>2</sup>/Hz was found for nBn devices at 100 Hz. This value lies on the dashed line in Fig. 5. Then,  $S_i \approx S_{bg}$  which implies  $S_{id} = S_i - S_{bg} \ll S_{bg}$  and so the estimation of detector noise at  $f = 100$  Hz is hardly possible. Contrary to this case, other measurements lie well above the limiting lines and estimation of detector noise is possible in these cases. For example, for an nBn device at  $T = 77$  K biased to  $U_D = -1.5$  mV the value  $S_i = 1.9 \times 10^{-26}$  A<sup>2</sup>/Hz was obtained using an amplifier gain of  $k_{iu} = 10^8$ . This value is roughly one order of magnitude higher than the background noise for this gain.

The above analysis was carried out for frequencies  $f > 100$  Hz. At lower frequencies  $S_{in}$  and  $S_{in}$  rise with decreasing frequency (see Fig. 4a) what raises also the limit for accurate measurement of detector's noise. Care must be taken also at frequencies above  $\sim 10^4$  Hz. In this case the condition  $|Z_{in}| \ll |Z|$  may not be fulfilled because the amplifier input impedance  $Z_{in}$  which increases with frequency and becomes comparable to the load impedance  $Z$  which decreases with  $f$  due to capacitive components of the device and test fixture. In general, capacitive loads may lead to amplifier instability what is prevented by the narrowing gain bandwidth. For the same reason measurements of large-capacitance loads with the EG&G 5182 unit in general should be avoided [15].

#### 4. Results and discussion

The psd of the detector noise current  $S_{id}$  is calculated by subtracting the background noise  $S_{bg}$  estimated according to (5) from the total measured noise  $S_i$ . A representative spectrum of nBn dark current noise is shown in Fig. 6a. Its shape is far from pure  $1/f$  dependence. It is disturbed by several Lorentzians, which contribute to the noise spectrum. Corner frequency  $f_c$  of the Lorentzian spectrum  $S_{id} \sim 1/(1+(f/f_c)^2)$  can be easily evaluated when the product  $fS_{id}$  is plotted versus frequency because in such representation a local maximum appears at the corner frequency. The plot in Fig. 6b allows to identify three Lorentzian contributions characterized by the corner frequencies  $f_c = 1.5, 80, 5850$  Hz.

More knowledge on random processes that produce Lorentzians can be gained from the inspection of the noise signal in the time domain. A time record in Fig. 7 collected with a digital scope reveals that the noise signal is non-Gaussian. Rather, amplitude quantization, characteristic for a random telegraph signal (RTS) can be observed. The 4-level signal in Fig. 7 can be produced by two RTSs with different time constants, which translate to different corner frequencies. Moreover, the amplitude of the “fast” process does not depend on the actual state of the „slow” process, which means that these RTSs are uncorrelated. Physically, an RTS can be produced in the two state system (TSS). In semiconductor devices a trap that exchanges the carrier with bands or other traps can form TSS. Traps can be located on device sidewalls or within the bulk. While the former is likely to occur in an nBn due to poor passivation of the detector mesa the latter are expected for a MCT diode as a large contribution of trap assisted tunneling current was identified in this device (Sec. 2). In a MCT diode, charge fluctuations in dislocation or at the surface region can also form TSSs. These fluctuations may couple to the electrical system through modulation of the width of the depletion region surrounding the dislocation core or the main diode depletion width [16].

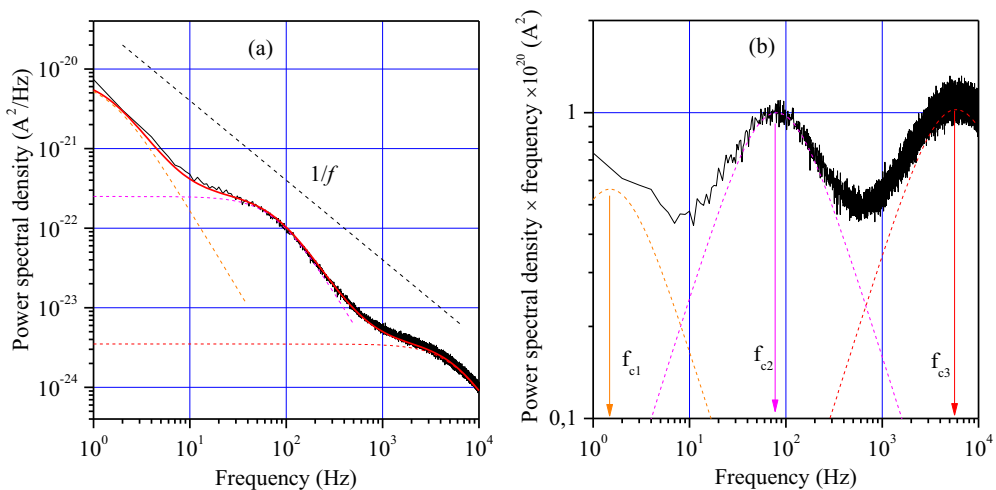


Fig. 6. Noise spectral density  $S_{id}$  (a) and the product  $fS_{id}$  (b) for reverse biased ( $U_D = -0,047$  V) nBn device at  $T = 77$  K (solid black lines). Lorentzian contributions are marked with dashed lines. Local maxima in (b) determine Lorentzian corner frequencies.

Dark current noise spectra of nBn detector and MCT diode taken for different reverse bias voltages are shown in Fig. 8. In general, for both devices an increase in the bias results in an increase of noise intensity. For the nBn detector the change of the bias affects not only  $1/f$  noise magnitude but also the shape of the spectrum: Lorentzians appear/disappear with the changing bias, which means that bias can turn on/off random processes produced in different TSSs. This is expected as quasi-Fermi level  $E_f$  moves with the bias and only traps above  $E_f$  can produce fluctuations. For the HgCdTe photodiode, the deviations of noise spectra from pure  $1/f$  shape are much lower. Small “bumps” overlaying the  $1/f$  dependency appear only in the bias range 48–640 mV. For both devices at the highest voltages the spectra become smoother and approach a regular  $1/f$  dependency. It is not clear whether Lorentzian contributions are all in the off state for these bias conditions or the structural  $1/f$  noise reaches a level that masks them.

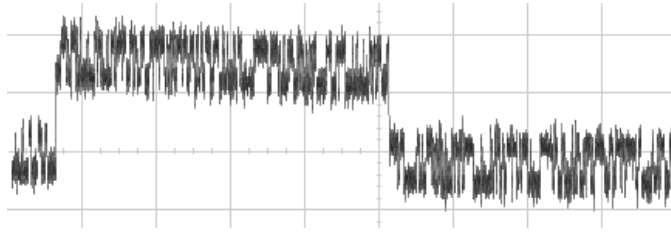


Fig. 7. Noise signal recorded for nBn detector at  $T = 83.4$  K reverse biased with  $U_D = -203$  mV. Oscilloscope time-base was 10 ms/div.

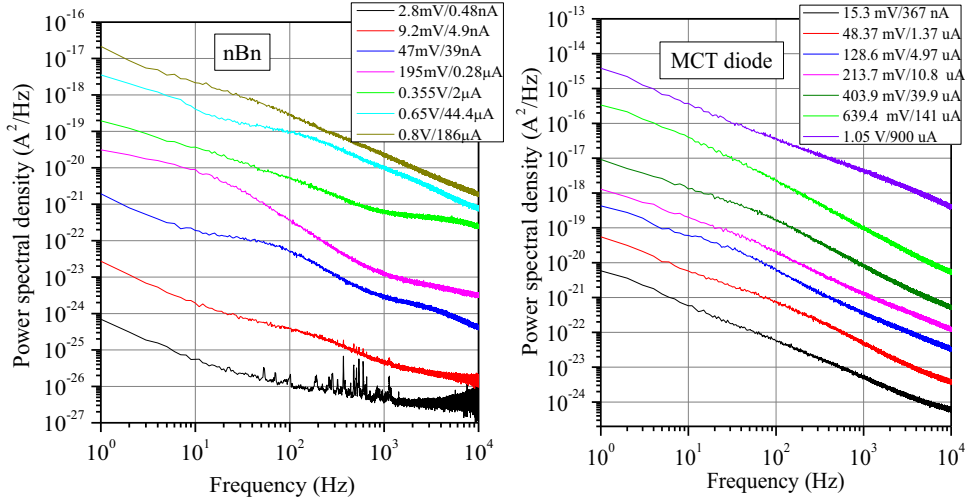


Fig. 8. Power spectral density of the current noise at 77 K for reversed biased nBn and MCT diode detectors. Curves from up to down refer to larger to lower bias.

Commonly used parameters characterizing  $1/f$  noise intensity are psd at 1 Hz,  $C \equiv S_{id}(f = 1$  Hz) and Hooge parameter  $\alpha$  that appears in the relation [17]

$$S_{id} = \frac{\alpha I_D^2}{Nf} = \frac{C}{f}, \quad (6)$$

which holds for ohmic devices. In (6)  $N$  is the number of free carriers in the noise producing volume. For nonlinear devices, a squared current dependence may not be justified so that parameter  $\alpha$  is expected to change with the bias. Moreover, the identification of the noise producing volume is not straightforward. When the spectrum deviates from an ideal  $1/f$  dependence, the parameter  $C$  is also not an adequate measure of noise intensity as slow Lorentzians may influence its value. Therefore, a better choice to estimate noise intensity is the use of noise power per frequency decade averaged over  $n$  decades

$$P_{dec} = \frac{1}{n} \int_{f_1}^{10^n f_1} S_{id}(f) df. \quad (7)$$

The values of  $P_{dec}$  for nBn and heterostructure detectors were calculated and are shown as a function of bias voltage in Fig. 9. We use this representation because voltage is the quantity that equally biases all parallel current paths. Consequently, the contributions to total noise that

can be different for different paths, can be better recognized. For this purpose, the measurements at 77 K are especially instructive. For small bias voltages, where ohmic leakage dominates (this region is experimentally best accessible at low temperatures - see Fig. 2a) the relation  $P_{\text{dec}} \sim U_D^2$  is observed (black lines in Fig. 9). In this region both samples are ohmic and quadratic dependence on bias voltage follows directly from (6). The contribution from leakage resistance noise at any bias voltage can be found by extrapolating a line drawn through the data in  $U_D \rightarrow 0$  limit to higher voltages. This line defines a reference minimum for all other noise. Contributions to the total noise connected with other currents (tunneling/diffusion/generation-recombination), which arise at larger bias, always increase noise power above this reference level.

In Fig. 9, apart from the 77 K series, data that summarize measurements at  $\sim 230\text{K}$  are also shown. With these data, a comparison of If performance of nBn and MCT devices can be made although it is not an easy task as the conclusions depend on the choice of the bias for operating conditions. MCT detectors usually operate with no bias so their If performance at 77 K is "leakage resistance noise limited". Quantitatively it can be described by the value of  $P_{\text{dec}}$  for the value of residual voltage that biases the detector in the readout circuitry. E.g.  $P_{\text{dec}} \approx 10^{-22}\text{A}^2$  for  $U_D = -1.6$  mV (see Fig. 9) which is the input offset voltage of the EG&G 5182 amplifier. For the same value of bias, the If performance of nBn is two orders of magnitude better ( $P_{\text{dec}} \approx 10^{-24}\text{A}^2$ ). However, nBn loses this superiority when biased to  $\sim -0.1$  V what is usually required for best operation. Then its If noise level at 77 K rises to  $P_{\text{dec}} \approx 2 \times 10^{-20}\text{A}^2$ .

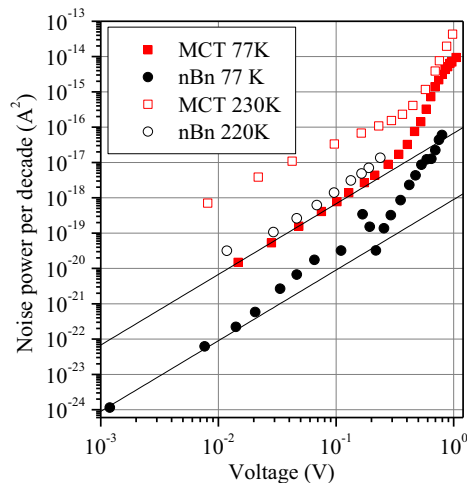


Fig. 9. Averaged power per decade of the low frequency noise  $P_{\text{dec}}$  calculated with formula (7) for nBn (points) and MCT detectors (squares) at 77 K (filled symbols) and 220 K/230 K (empty symbols) as a function of bias voltage. Black solid lines have the slope of two.

At temperatures  $\sim 230$  K useful for HOT devices our data reveal that If noise of MCT detectors is more than one order of magnitude higher than that of nBn's if referred to the same bias voltage. Large  $1/f$  noise found in the MCT detector is a known fact, which in principle was the reason for not using these devices with nonzero bias [7]. We may estimate e.g. that an attempt to use non-equilibrium detection at  $U_D = -0.23\text{V}$  where  $RA$  reaches maximum ( $R = 21$  k $\Omega$ ) would produce If noise of  $P_{\text{dec}} \approx 10^{-16}\text{A}^2$  which corresponds to noise current density  $I_d \approx (P_{\text{dec}}/\ln(10)/f)^{1/2} = 6.6$  nA/Hz $^{1/2}$  @  $f = 1$  Hz and  $1/f$ -to-shot-noise onset at  $f_{\text{knee}} = P_{\text{dec}}/(\ln(10)2qI_D) \approx 2.8$  MHz as dc current  $I_D = 49$   $\mu\text{A}$  flows for this bias. On the contrary, a

nonbiased MCT detector is limited by its thermal noise of  $\approx 4.5 \text{ pA/Hz}^{1/2}$ . When a nBn detector is biased to  $U_D = -0.135\text{V}$  where  $RA$  reaches a maximum ( $R = 500 \Omega$ ) its  $1/f$  noise of  $P_{\text{dec}} \approx 3 \times 10^{-18} \text{ A}^2$  corresponds to a noise current of  $I_d \approx 0.9 \text{ nA/Hz}^{1/2}$  @  $1\text{Hz}$  and  $f_{\text{knee}} \approx 6 \text{ kHz}$  as  $I_D = 0.67 \text{ mA}$  at this bias. Due to low  $R_0$ -value of  $\sim 60 \Omega$  the nonbiased nBn detector is amplifier + thermal noise limited. For best instruments with equivalent input noise voltage of  $u_n = 1 \text{ nV/Hz}^{1/2}$  this limitation gives a noise current of  $\approx 22 \text{ pA/Hz}^{1/2}$  above amplifier's  $1/f$  frequency knee which typically is  $> 10 \text{ Hz}$  (see e.g. Fig. 4a). Therefore, good  $1/f$  performance of nBn is lost due to its low resistance.

We may summarize that in HOT conditions,  $1/f$  performance of biased nBn ( $0.9 \text{ nA/Hz}^{1/2}$ ) is better than biased MCT photodiode ( $6.6 \text{ nA/Hz}^{1/2}$ ) however, it is much poorer if compared to a nonbiased MCT device ( $< 66 \text{ pA/Hz}^{1/2}$ ). Nonbiased nBn suffers significantly from its low resistance, which gives not only a low  $R_0A$  product but also makes the detection amplifier and/or thermal noise limited. In addition, nonbiased nBn has low sensitivity.

## 5. Summary

In the transimpedance detection system the instrumental background noise depends not only on amplifier internal noise but also on the dynamic resistance of the device under test and impedance of the environmental circuitry. Proper evaluation of this noise is an important issue since it can give a significant contribution to the total measured noise. In general,  $1/f$  noise spectra of T2SL nBn and heterostructure photodiode MCT detectors are of  $1/f$  type, however nBn noise spectra include Lorentzian inclusions. For a small bias in both devices,  $1/f$  noise is connected with fluctuations of the leakage resistance. These fluctuations define a lower limit of the  $1/f$  noise in these devices. Additional dark current components lead to an increase of  $1/f$  noise intensity above this limit. A T2SL nBn detector has better  $1/f$  performance than a heterostructure MCT detector when both are biased to the same voltage. However, in practical HOT implementations the  $1/f$  performance of a nonbiased MCT detector is still much better than that of T2SL barrier devices.

## References

- [1] Martyniuk, P., Wróbel, J., Plis, E., Madejczyk, P., Kowalewski, A., Gawron, W., Krishna, S., Rogalski, A. (2012). Performance modeling of MWIR InAs/GaSb/B-Al<sub>0.2</sub>Ga<sub>0.8</sub>Sb type-II superlattice nBn detector. *Semicond. Sci. Technol.*, vol. 27, 055002.
- [2] Cowan, V. M., Morath, C. P., Myers, S., Gautam, N., Krishna, S. (2011). Low temperature noise measurement of an InAs/GaSb-based nBn MWIR detector. *Infrared Technology and Applications*, vol. 8012, 801210.
- [3] Wörl, A., Kleinow, P., Rehm, R., Schmitz, J., Walther, M. (2013). Noise characteristics of InAs/GaSb superlattice infrared photodiodes. *Phys. Status Solidi C*, 10, 744–747.
- [4] Kim, H. S., Plis, E., Gautam, N., Myers, S., Sharma, Y., Dawson, L. R., Krishna, S. (2010). Reduction of surface leakage current in InAs/GaSb strained layer longwavelength superlattice detectors using SU-8 passivation. *Appl. Phys. Lett.*, 97, 143512.
- [5] Rodriguez, J. B., Plis E., Bishop G., Sharma Y. D., Kim H., Dawson L. R., Krishna, S. (2007). nBn structure based on InAs/GaSb type-II strained layer superlattices. *Appl. Phys. Lett.*, 91, 043514.
- [6] Gopal, V., Plis, E., Rodriguez, J.-B., Jones, C. E., Faraone, L., Krishna, S. (2008). Modeling of electrical characteristics of midwave type II InAs/GaSb strain layer superlattice diodes. *Journal of Applied Physics*, 104, 124506.
- [7] Piotrowski, J., Piotrowski, A. (2011). Room temperature photodetectors. *Mercury Cadmium Telluride: Growth, Properties and Applications* edited by Capper P. and James Garland, Wiley, 513–537.

- [8] Soibel, A., Nguyen, J., Höglund, L., Hill, C. J., Ting, D. Z., Keo, S. A., Mumolo, J. M., Lee, M. C., Gunapala, S. D. (2011). InAs/GaSb superlattice based long-wavelength infrared detectors: Growth, processing, and characterization. *Infrared Physics & Technology*, 54, 247–251.
- [9] Gopal, V., Gupta, S. (2006). Contribution of dislocations to  $1/f$  noise in mercury cadmium telluride infrared photovoltaic detectors. *Infrared Physics & Technology*, 48, 59–66.
- [10] Johnson, S. M., Rhiger, D. R., Rosbeck, J. P., Peterson, J. M., Taylor, S. M. (1992). Effect of dislocations on the electrical and optical properties of long wavelength infrared HgCdTe photovoltaic detectors. *J. Vac. Sci. Technol.*, B 10, 1499.
- [11] Józwickowski, K., Józwickowska, A., Koptyko, M., Rogalski, A., Jaroszewicz, L. R. (2012). Simplified model of dislocations as a SRH recombination channel in the HgCdTe heterostructures. *Infrared Physics & Technology*, 55(1), 98–107.
- [12] Elliott, C. T., Gordon, N. T., Hall, R. S., Phillips, T. J. (1997).  $1/f$  Noise Studies in Uncooled Narrow Gap Hg<sub>1-x</sub>Cd<sub>x</sub>Te Non-Equilibrium Diodes. *Journal of Electronic Material*, vol. 26, 6, 643-648.
- [13] Rais, M. H., Musca, C. A., Dell, J. M., Antoszewski, J., Nener, B. D., Faraone, L. (2000). Photovoltaic detectors fabricated using a new junction formation technology. *Microelectronics Journal*, 31, 545–551.
- [14] Juang, F. S., Su, Y. K., Chang, S. J., Chang, S. M., Shu, F. S., Chiang, C. D., Cherng, Y. T., Sun, T. P. (1999). Dark Currents in HgCdTe Photodiodes Passivated with ZnS/CdS. *Journal of the Electrochemical Society*, 146 (4), 1540-1545.
- [15] Transimpedance amplifier EG&G 5182. Instruction manual. (January 2014). <http://www.signalrecovery.com>.
- [16] Kinch, M. A., Strong, R. L., Schaake, C. A. (2013).  $1/f$  Noise in HgCdTe Focal-Plane Arrays. *Journal of Electronic Material*, vol. 42, 11, 3243-3251.
- [17] Hooge, F. N., Klainpenning, T. G. M., Vandamme, L. K. J. (1981). Experimental studies on  $1/f$  noise. *Rep. Prog. Phys.*, vol. 44, 479.